Progress In Electromagnetics Research M, Vol. 83, 151–159, 2019

Single-Fed High-Gain Circularly Polarized Microstrip Antenna

Qing-Qing Chen, Jian-Ying Li, Guang-Wei Yang*, and Yu-Xin Ding

Abstract—In this paper, a single-fed high-gain circularly polarized microstrip antenna is proposed. The circular polarization is obtained by two unequal-length arc-shaped radiation patches, which excite two orthogonal linearly polarized modes with a 90° phase difference. The antenna is excited by coaxial feed. The proposed circularly polarized antenna consists of two arc-shaped radiation patches and a ground plane, which has a simple structure and a higher gain than 10.0 dB. The antenna is fabricated and measured to verify the design. The measured results are in good agreements with the simulated ones. The measured results show that the impendence bandwidth (IBW) for $S_{11} < -10$ dB is 16.7% (3.78–4.47 GHz), and the axial-ratio bandwidth (ARBW) for AR < 3 dB is 3.6% (4.09–4.24 GHz). Further, the gain is higher than 10.0 dB from 4.09 to 4.24 GHz. The antenna radiation pattern performs well over the whole band, and the peak gain can reach 10.67 dB at 4.11 GHz. It is a good candidate for advanced wireless communication systems.

1. INTRODUCTION

Circularly polarized (CP) microstrip antennas are widely used in radar, navigation, and satellite communication realms owing to their small size, low profile, great flexibility, and many other advantages [1]. Circular polarization is produced by using the feeding structure to excite two orthogonal linearly polarized modes with a 90° phase difference [2–13]. A single-fed circularly polarized patch antenna can be designed by slotting or chamfering on a square patch [2–4]. For these single-fed patch antennas, the measured −10 dB return loss bandwidth and 3 dB axial ratio bandwidth are less than 5% and 2%, respectively. Circular polarization can also be obtained by a ring antenna with an asymmetrical structure [5–8]. When operated in the fundamental mode, the size of the annular ring patch antenna is smaller than that of the circular or rectangular patch for a given frequency. Reference [5] presents a circularly polarized annular-ring patch antenna achieved by a simple microstrip feed line through the coupling of a fan-shaped patch on the same plane of the antenna. The impendence bandwidth (IBW) is 2.3% (2.68 ∼ 2.74 GHz), and axial-ratio bandwidth (ARBW) is 0.6% (2.69 ∼ 2.71 GHz). In [6], a circularly polarized cut ring microstrip antenna is proposed, and the measured ARBW is 4.2%. A novel miniaturized CP implantable annular-ring antenna is proposed in [7], which has 2.49% ARBW. Reference [8] proposes a polarization-reconfigurable antenna based on ring circularly polarized microstrip antenna. The IBW is 16.7%, and the ARBW is 3.2%. Some structures, which enhance the bandwidth of single-fed circularly polarized patch microstrip antennas, are studied [9–11]. Reference [9] designs a circularly polarized antenna composed of a U-slot square patch with truncated corners supported by a substrate with dielectric constant of 10.02. A measured IBW of 15.2% (1.53 ∼ 1.78 GHz) and ARBW of 3.2% (1.56 ∼ 1.61 GHz) is achieved. A circularly polarized single-layer asymmetrical U-slot microstrip patch antenna is proposed in [10]. The asymmetrical structure of the U-slot provides two different current paths for the two orthogonal modes required for circular polarization. The measured

Received 20 May 2019, Accepted 19 July 2019, Scheduled 7 August 2019

* Corresponding author: Guang-Wei Yang (guangweiyang@mail.nwpu.edu.cn).
The authors are with the School of Electronics and Information, Northwestern Polytechnical University, No. 127, Youyi Road (West), Beilin, Xi'an, China.

impedance bandwidth ($S_{11} < 10\,\text{dB}$) and 3-dB axial ratio bandwidth of the antenna are about 9.0% and 4.0%, respectively. Reference [11] finds that the bandwidth of a circularly polarized microstrip antenna can be enhanced by using two annular-sector-shaped parasitic patches. Much wider impedance and AR bandwidth can be achieved for dual-feeds [12, 13] and multiple linearly polarized radiating elements [14]. However, an additional feeding network is required which results in huge volume. Linearly polarized wave is converted to circularly polarized waves by using a metasurface (MS) structure [15–17], whose 3-dB axial bandwidth is wider than 10%.

In this paper, a novel single-fed high-gain circularly polarized microstrip antenna with a different circularly polarized radiation mechanism from the antenna in [6] is proposed. The circular polarization is obtained by two arc-shaped radiation patches of unequal length. Compared with conventional microstrip antenna with a substrate, the advantage of the proposed structure as a circularly polarized antenna is the high gain which is due to less amount of stored energy under the metalized patch. Table 1 shows a comparison of the proposed antenna with other single-fed circularly polarized microstrip antennas [2, 3, 5, 6, 8–11] presented in recent literature. The comparison shows that this antenna has a higher gain.

Table 1. Comparison of single-fed CP microstrip antennas.

Ref.	Size (mm^3), $\lambda = c/f_{Low}$	$S_{11} < -10\,\text{dB}$, BW (%, GHz)	AR $< 3\,\text{dB}$, BW (%, GHz)	Peak Gain (dBi)
[2]	$0.14\lambda \times 0.14\lambda \times 0.02\lambda$	4.3 (2.362–2.466)	1.0 (2.403–2.427)	4.21
[3]	$0.24\lambda \times 0.24\lambda \times 0.03\lambda$	5.0 (1.545–1.625)	1.6 (1.56–1.585)	5.20
[5]	$\Phi 0.13\lambda \times 0.03\lambda$	2.3 (2.68–2.74)	0.6 (2.69-2.71)	3.50
[6]	$\Phi 0.57\lambda \times 0.06\lambda$	19.3 (2.95-3.58)	4.2 (3.31–3.46)	10.97
[8]	$\Phi 0.52\lambda \times 0.07\lambda$	16.7 (3.70–4.37)	3.2 (3.95–4.08)	10.60
[9]	$0.13\lambda \times 0.13\lambda \times 0.05\lambda$	15.1 (1.53–1.78)	3.2 (1.56–1.61)	4.50
[10]	$0.34\lambda \times 0.34\lambda \times 0.08\lambda$	9.0 (2.27–2.48)	4.0 (2.27–2.36)	8.17
[11]	$\Phi 0.5\lambda \times 0.02\lambda$	6.0 (2.93–3.11)	3.3 (3.00–3.10)	2.70
Prop.	$\Phi 0.55\lambda \times 0.05\lambda$	18.2 (3.80–4.56)	4.1 (4.09–4.26)	11.02

This paper is organized as follows. Section 1 provides an introduction to the research on single-fed circularly polarized microstrip antennas. Section 2 describes and analyzes the design of the proposed single-fed circularly polarized microstrip antenna. Section 3 presents the simulated and measured results for the designed antenna. Section 4 provides the study conclusions.

2. ANTENNA DESIGN AND ANALYSIS

2.1. Antenna Design

The goal of this paper is to design a single-fed high-gain circularly polarized microstrip antenna. Fig. 1 shows the geometry, top view, and side view of the proposed antenna, which has a center frequency of 4.2 GHz. The antenna consists of two unequal-length arc-shaped radiation patches, and the thickness is $H_2 = 1\,\text{mm}$. The inner radius and outer radius of the two arc-shaped patches are R_1 and R_2, respectively, which are fixed by using four non-metallic nylon columns. R_5 and θ_3 determine the position of the supporting columns. An air layer, which is 4.0 mm (H_1), is loaded between the radiation patch and ground plane. In addition, a radial fan-shaped slot of angle θ_1 is reserved on the forth quadrant of the radiation plane. With the presence of two unequal-length arc-shaped patches, two orthogonal linearly polarized modes with a 90° phase difference is excited to obtain circularly polarized characteristics from 4.09 to 4.26 GHz. The antenna is excited by coaxial feed, and R_3 illustrates the feed point position.

To explain the design process of this circularly polarized antenna clearly, three steps depicting the evolution structure are shown in Fig. 2 (Antennas 1–3). The antenna simulation is conducted with the High Frequency Simulation Software (HFSS) [18]. Antenna 1 includes only a circular metal patch, which radiates LP. The desired value of R_1 at the operating frequency is obtained from Eq. (1), that

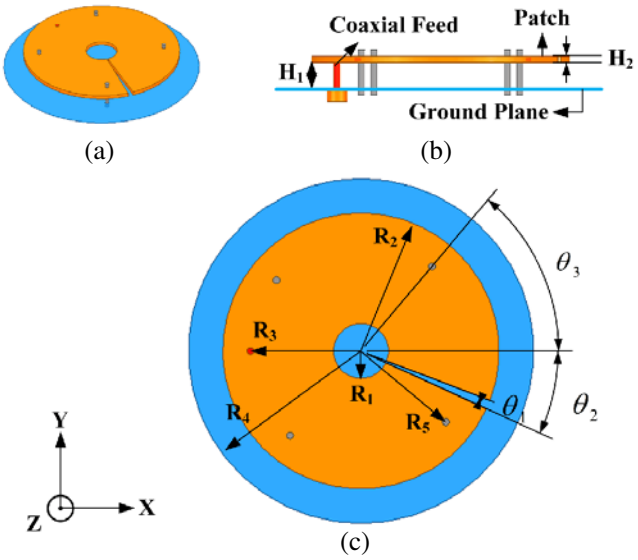

Figure 1. Geometry of the proposed antenna (mm). (a) 3-D view. (b) Side view. (c) Top view. $R_1 = 4.0$, $R_2 = 20.0$, $R_3 = 16.0$, $R_4 = 55.0$, $R_5 = 16.0$, $H_1 = 4.0$, $H_2 = 1.0$, $\theta_1 = 4°$, $\theta_2 = 25°$ and $\theta_3 = 50°$.

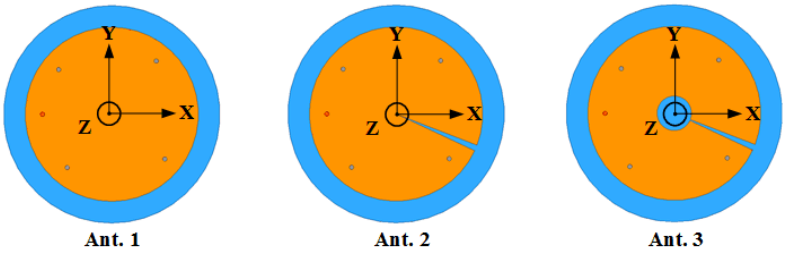

Figure 2. Three improved prototypes of the proposed CP antenna.

is [19],

$$R_1 = \frac{8.794}{f_0\sqrt{\varepsilon_{eff}}}\,\text{cm} \tag{1}$$

f_0 is given in GHz, and ε_{eff} is the effective dielectric constant. Antenna 1 operates at the center frequency of 4.1 GHz, and the estimated R_1 is about 18.7 mm, which is close to the simulated value ($R_1 = 20.0$ mm). Based on Antenna 1, a radial slot (θ_1) is etched on the forth quadrant of the radiation plane in Antenna 2. Since the radial slot perturbs the current along the slot, the excited y-directed surface current path is lengthened, while the excited x-directed current is slightly affected. Hence the CP can be achieved due to the combination of an almost unchanged mode with the new resonance mode excited along y-direction. A concentric circle is etched in Antenna 3 to improve the impedance matching of the CP antenna. The S_{11} and AR of the three antennas are depicted in Fig. 3. Antenna 1 is an LP antenna. Antenna 2 can radiate CP as a new resonant mode is excited by the radial slot. However, at lower operating frequency, impedance matching is good, but the AR is bad, while at higher operating frequency, the AR is improved, but the impedance matching is deteriorated. The impedance matching of Antenna 3 is improved. The IBW for $S_{11} < -10$ dB is 18.2% (3.80–4.56 GHz), and the ARBW for AR < 3 dB is 4.1% (4.09–4.26 GHz).

To illustrate the CP operation mechanism of the proposed antenna, Fig. 4 depicts the surface current distributions at 4.2 GHz for four phases of 0°, 90°, 180°, and 270°. The predominant surface current in the azimuth plane rotates clockwise, which is accountable for left-hand circular polarization (LHCP).

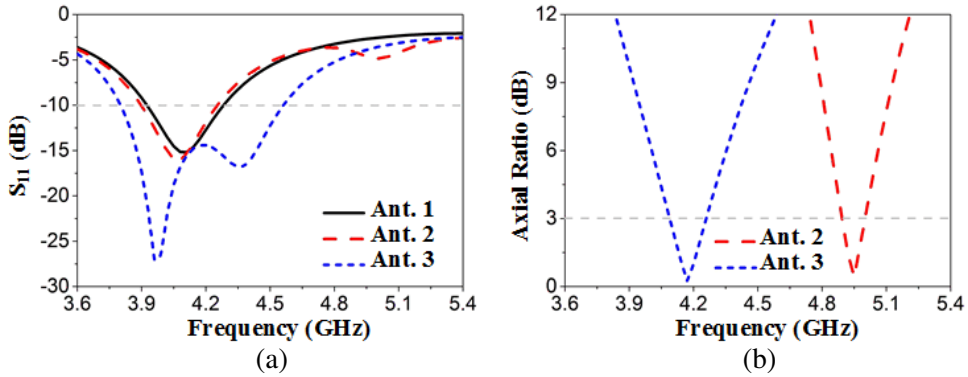

Figure 3. Simulated S_{11} and AR for Ants. 1–3. (a) S_{11}, (b) AR.

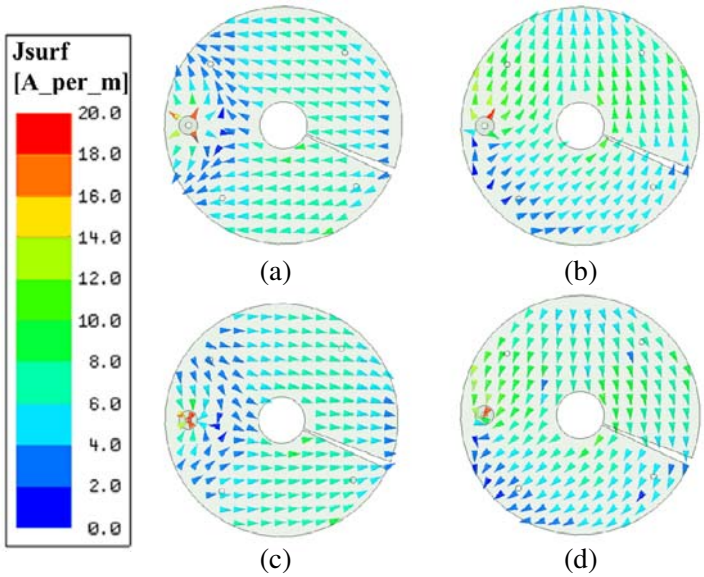

Figure 4. Simulated surface current distributions of the proposed antenna at 4.2 GHz: (a) $t = 0$, (b) $t = T/4$, (c) $t = T/2$, (d) $t = 3T/4$.

2.2. Parameters Studies

To describe the performance of the proposed antenna clearly, some key parameters of the designed antenna are discussed. The performance of the proposed antenna is determined by several important parameters, including the angle of the radial fan-shaped slot (θ_1), the height of the air layer (H_1), the position of the fan-shaped radial slot (θ_2), the position of the coaxial feed (R_3), and the thickness of patch (H_2).

The first parameter studied is θ_1, which has a considerable effect on the impedance matching and axial ratio of the antenna. According to the simulated data shown in Fig. 5, the impedance bandwidth of the antenna extends as θ_1 increasing from 2° to 5°. However, when θ_1 is 5°, S_{11} deteriorates markedly at middle frequency (4.2 GHz). When θ_1 is increased, the operating frequency of the AR clearly shifts to a higher frequency. AR provides the best performance when θ_1 is 4°. The influence of θ_1 on the antenna is consistent with the antenna design theory.

The second parameter investigated is the height of the air layer (H_1). In the simulation results shown in Fig. 6, both S_{11} and AR curves shift to a lower frequency as the height of the air layer changes from 3 mm to 4.5 mm. The S_{11} curve deteriorates at lower frequencies, and the AR deteriorates markedly at the entire operating frequencies when the height is 3 mm. The proper height is 4 mm,

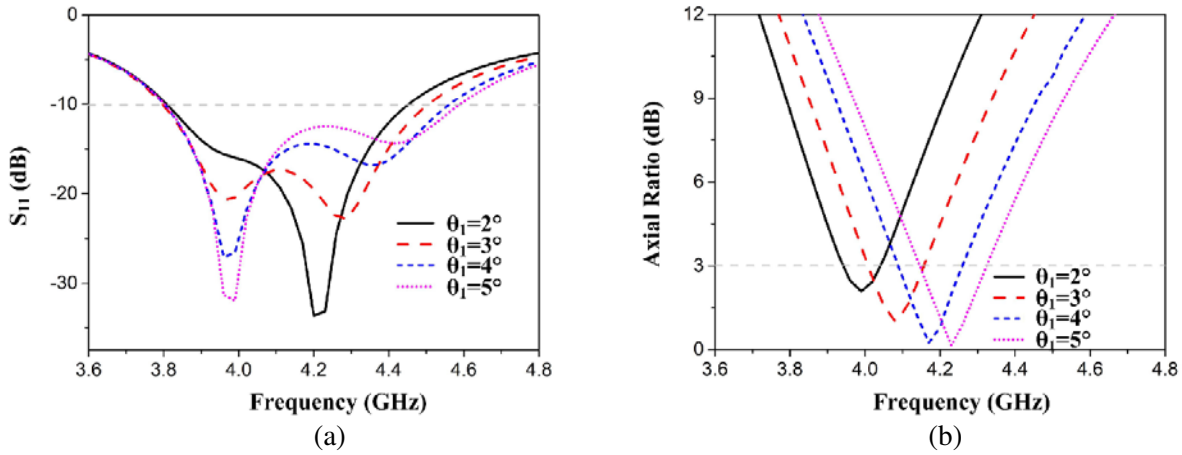

Figure 5. Effects of various θ_1 on S_{11} and AR (mm). (a) S_{11}, (b) AR. R_1=4.0, $R_2 = 20.0$, $R_3 = 16.0$, $R_4 = 55.0$, $R_5 = 16.0$, $H_1 = 4.0$, $H_2 = 1.0$, $\theta_2 = 25°$, and $\theta_3 = 50°$.

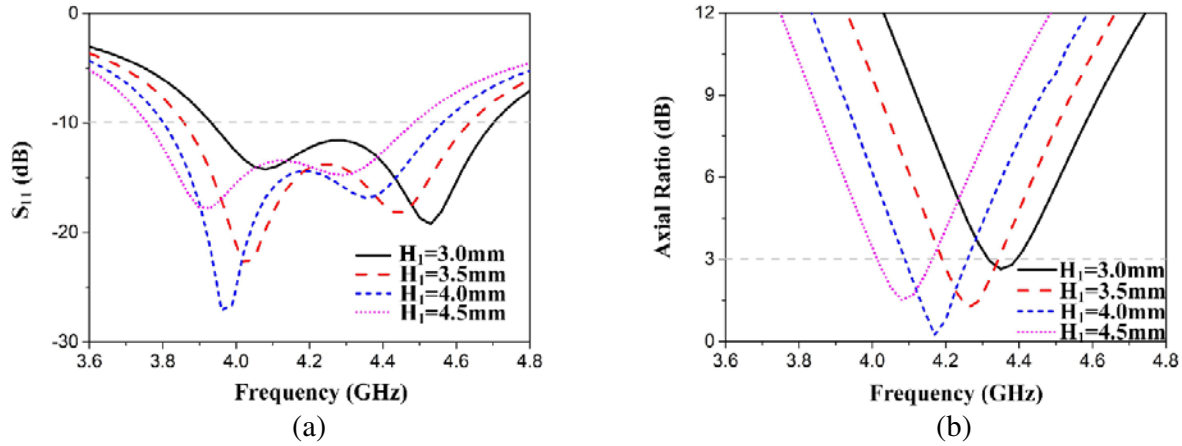

Figure 6. Effects of various H_1 on S_{11} and AR (mm). (a) S_{11}, (b) AR. $R_1 = 4.0$, $R_2 = 20.0$, $R_3 = 16.0$, $R_4 = 55.0$, $R_5 = 16.0$, $H_2 = 1.0$, $\theta_1 = 4°$, $\theta_2 = 25°$, and $\theta_3 = 50°$.

at which the impedance matching is good, and the AR provides the best performance at the entire operating frequencies.

The third parameter studied is the position of the fan-shaped radial slot (θ_2). Fig. 7 shows the influence of the position of the slot on the performance of the antenna. The simulated data indicate that θ_2 mainly affects the antenna impedance bandwidth and has little effect on the AR. When θ_2 is 23°, the impedance bandwidth is narrowed. On the contrary, when θ_2 increases to 29°, the S_{11} deteriorates considerably at middle frequency (4.2 GHz). When θ_2 has a proper value (25°), S_{11} performs well.

The fourth studied parameter is the position of feeding (R_3). According to the simulated data in Fig. 8, R_3 has great influence on S_{11}. The resonance of S_{11} clearly shifts to a higher frequency as R_3 increasing from 12.0 mm to 18.0 mm. S_{11} deteriorates markedly at higher frequencies when R_3 is 12.0 mm. As R_3 increases to 16.0 mm, S_{11} is improved. To achieve the best impedance matching performance, R_3 is selected to be 16.0 mm.

The last studied parameter is the thickness of patch (H_2), which has a considerable effect on the axial ratio and impedance matching. According to the simulated data in Fig. 9, the operating frequency of the designed antenna clearly shifts to a lower frequency as H_2 increasing from 0.5 mm to 2.0 mm. When H_2 is selected to be 1.0 mm, the circularly polarized performance is the best, and the impedance matching is less than −10 dB over the operating bandwidth.

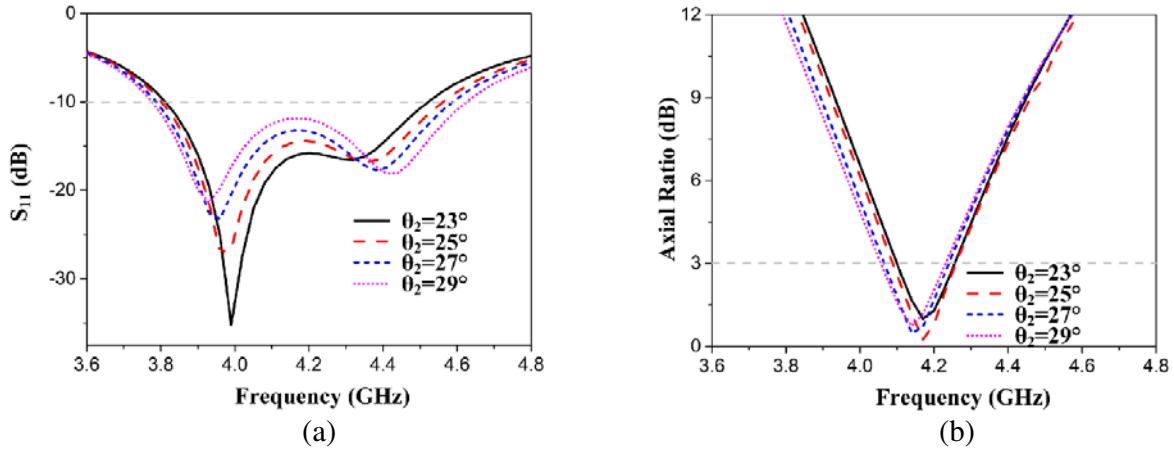

Figure 7. Effects of various θ_2 on S_{11} and AR (mm). (a) S_{11}, (b) AR. $R_1 = 4.0$, $R_2 = 20.0$, $R_3 = 16.0$, $R_4 = 55.0$, $R_5 = 16.0$, $H_1 = 4.0$, $H_2 = 1.0$, $\theta_1 = 4°$, and $\theta_3 = 50°$.

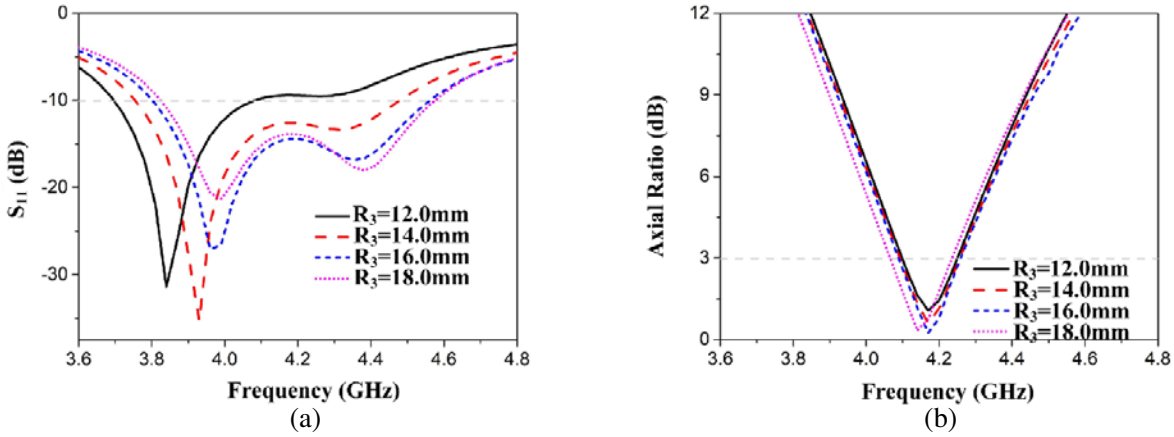

Figure 8. Effects of various R_3 on S_{11} and AR (mm). (a) S_{11}, (b) AR. R_1=4.0, $R_2 = 20.0$, $R_4 = 55.0$, $R_5 = 16.0$, $H_1 = 4.0$, $H_2 = 1.0$, $\theta_1 = 4°$, $\theta_2 = 25°$, and $\theta_3 = 50°$.

3. EXPERIMENTAL RESULTS

The antenna is fabricated based on optimized design parameters. The antenna prototype is tested using the vector network analyzer ROHDE&SCHWARZ ZVB20 [20] and the Near Field Antenna Measurement System, which estimates far-field radiation performance by collecting near-field data. Fig. 10 shows photographs of the antenna, and Fig. 11 presents both the measured and simulated values of S_{11}, AR, and gain. The measured results agree well with the simulated ones and are slightly shifted to lower frequencies. The measured IBW for $S_{11} < -10$ dB is 16.7% (3.78–4.47 GHz), whereas the simulated bandwidth is 18.2% (3.80–4.56 GHz). Due to the deviation for fabricating antenna, the simulated result has higher Q-factor considering the measured result. The 3-dB axial ratio bandwidth is roughly 3.6% (4.09–4.24 GHz) with center frequency at 4.2 GHz for LHCP. The designed antenna provides a very high gain, more than 10.0 dB at the whole operating bandwidth (4.09–4.24 GHz). The peak gain can reach 10.67 dB at 4.11 GHz. The simulated antenna efficiency of the designed antenna is shown in Fig. 12(a). It shows that the antenna efficiency is higher than 90% within the operating frequency band. The good directivity of the proposed antenna could be obtained by the ratio of realized gain to the efficiency.

Figure 12(b) shows the simulated and measured radiation patterns in xz-plane and yz-plane at 4.2 GHz. The antenna radiation patterns are consistent with the analysis results on the antenna surface current distribution, which is shown in Fig. 4. LHCP radiations are achieved. The radiation

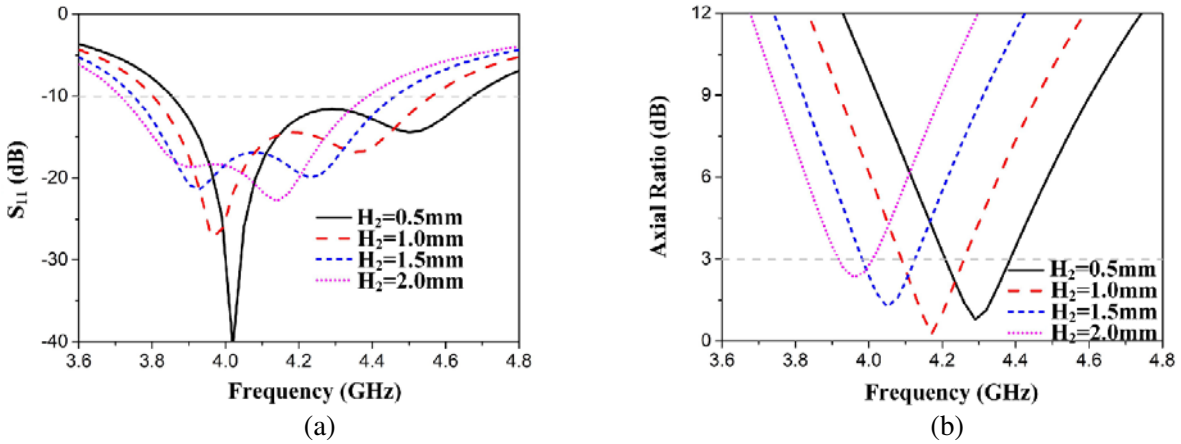

Figure 9. Effects of various H_2 on S_{11} and AR (mm). (a) S_{11}, (b) AR. $R_1 = 4.0$, $R_2 = 20.0$, $R_3 = 16.0$, $R_4 = 55.0$, $R_5 = 16.0$, H_1=4.0, $\theta_1 = 4°$, $\theta_2 = 25°$ and $\theta_3 = 50°$.

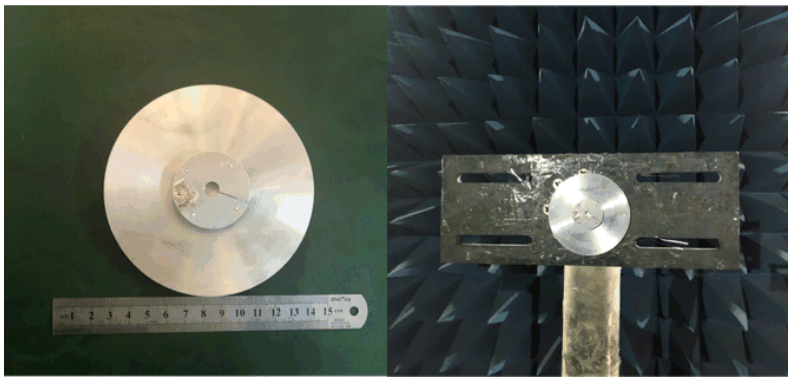

Figure 10. Photographs of proposed antenna.

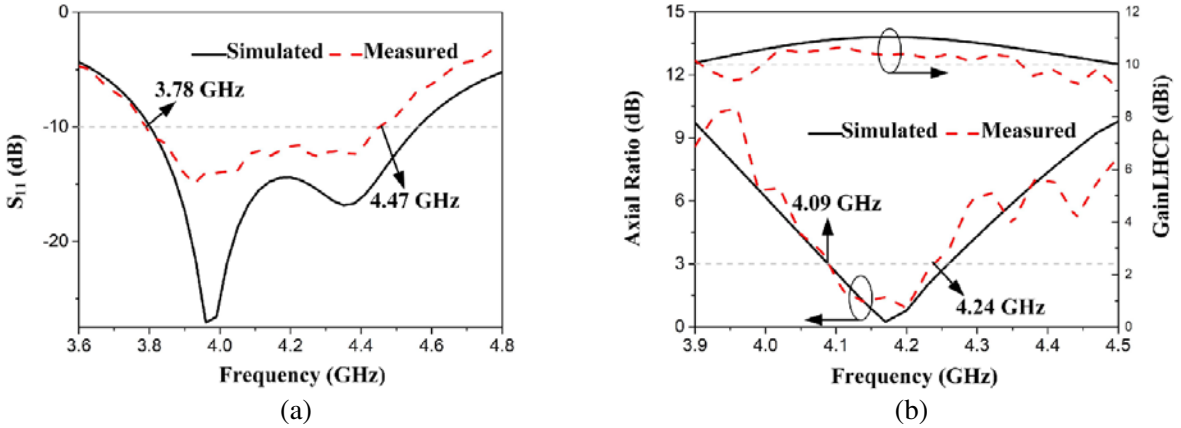

Figure 11. Simulated and measured S_{11}, AR, and antenna gain of proposed antenna. (a) S_{11}, (b) AR and antenna gain.

patterns under test and simulation results are shown to be basically identical. A co-polarization/cross-polarization ratio of better than 20 dB is observed in all of the measured radiation patterns, indicating excellent polarization purity.

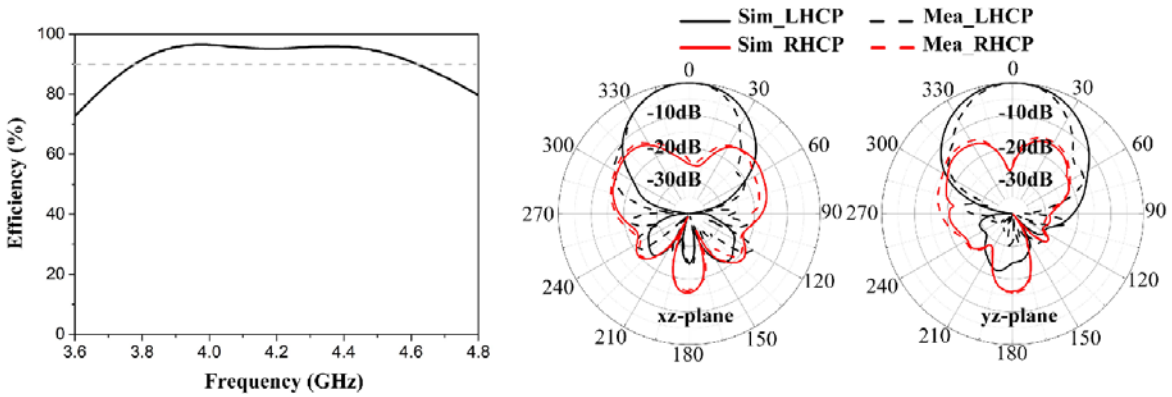

Figure 12. Simulated antenna efficiency and measured radiation patterns of proposed antenna at 4.2 GHz. (a) Antenna efficiency, (b) radiation patterns.

4. CONCLUSION

A single-fed high-gain circularly polarized microstrip antenna has been investigated for wireless communication. The circular polarization is obtained by two unequal-length arc-shaped radiation patches. The proposed antenna has a pretty simple structure and higher gain than 10.0 dB. The measured IBW for $S_{11} < -10$ dB is 16.7% (3.78–4.47 GHz), and 3-dB axial ratio bandwidth is roughly 3.6% (4.09–4.24 GHz) with center frequency at 4.2 GHz for LHCP. The designed antenna provides a very high gain more than 10.0 dB at the whole operating bandwidth (4.09–4.24 GHz). The peak gain can reach 10.67 dB at 4.11 GHz. It is a good candidate for advanced wireless communication systems.

REFERENCES

1. Xu, Y., S. Gong, and T. Hong, "Circularly polarized slot microstrip antenna for harmonic suppression," *IEEE Antennas and Wireless Propagation Letters*, Vol. 12, 472–475, 2013.
2. Hong, T., S. Gong, Y. Liu, W. Jiang, and J. Du, "Miniaturized circularly polarized microstrip antenna by spirally slotted," *2015 IEEE 4th Asia-Pacific Conference on Antennas and Propagation (APCAP)*, 585–586, Kuta, 2015.
3. Nasimuddin, X. Qing, and Z. N. Chen, "Circularly polarized ring-slotted-microstrip antenna," *2015 IEEE 4th Asia-Pacific Conference on Antennas and Propagation (APCAP)*, 203–204, Kuta, 2015.
4. Huo, X. Y., J. H. Wang, and M. E. Chen, "Circularly polarized microstrip antenna with two Asymmetric Circular slots for RFID application," *2013 IEEE International Conference on Microwave Technology & Computational Electromagnetics*, 184–187, Qingdao, 2013.
5. Lin, Y., H. Chen, and S. Lin, "A new coupling mechanism for circularly polarized annular-ring patch antenna," *IEEE Transactions on Antennas and Propagation*, Vol. 56, No. 1, 11–16, Jan. 2008.
6. Yang, Y., J.-Y. Li, K. Wei, R. Xu, and G.-W. Yang, "Circularly polarised cut ring microstrip antenna," *Electronics Letters*, Vol. 51, No. 3, 199–200, 2015.
7. Li, R., Y. Guo, B. Zhang, and G. Du, "A miniaturized circularly polarized implantable annular-ring antenna," *IEEE Antennas and Wireless Propagation Letters*, Vol. 16, 2566–2569, 2017.
8. Chen, Q., J. Li, G. Yang, B. Cao, and Z. Zhang, "A polarization-reconfigurable high-gain microstrip antenna," *IEEE Transactions on Antennas and Propagation*, Vol. 67, No. 5, 3461–3466, May 2019.
9. Lam, K. Y., K. Luk, K. F. Lee, H. Wong, and K. B. Ng, "Small circularly polarized u-slot wideband patch antenna," *IEEE Antennas and Wireless Propagation Letters*, Vol. 10, 87–90, 2011.
10. Tong, K. and T. Wong, "Circularly polarized U-slot antenna," *IEEE Transactions on Antennas and Propagation*, Vol. 55, No. 8, 2382–2385, Aug. 2007.

11. Lin, J. and Q. Chu, "Enhancing bandwidth of CP microstrip antenna by using parasitic patches in annular sector shapes to control electric field components," *IEEE Antennas and Wireless Propagation Letters*, Vol. 17, No. 5, 924–927, May 2018.
12. Bilotti, F. and C. Vegni, "Design of high-performing microstrip receiving GPS antennas with multiple feeds," *IEEE Antennas and Wireless Propagation Letters*, Vol. 9, 248–251, 2010.
13. Chen, X., G. Fu, S. Gong, Y. Yan, and W. Zhao, "Circularly polarized stacked annular-ring microstrip antenna with integrated feeding network for UHF RFID readers," *IEEE Antennas and Wireless Propagation Letters*, Vol. 9, 542–545, 2010.
14. Zhang, B., Y. P. Zhang, D. Titz, F. Ferrero, and C. Luxey, "A circularly-polarized array antenna using linearly-polarized sub grid arrays for highly-integrated 60-GHz radio," *IEEE Transactions on Antennas and Propagation*, Vol. 61, No. 1, 436–439, Jan. 2013.
15. Altintas, O., E. Unal, O. Akgol, M. Karaaslan, and F. Karadag, "Design of a wide band metasurface as a linear to circular polarization converter," *Modern Physics Letters B*, Vol. 31, No. 30, 2017.
16. Akgol, O., O. Altintas, E. Unal, M. Karaaslan, and F. Karadag, "Linear to left- and right-hand circular polarization conversion by using a metasurface structure," *International Journal of Microwave and Wireless Technologies*, Vol. 10, No. 1, 133–138, 2018.
17. Akgol, O., E. Unal, O. Altintas, M. Karaaslan, and F. Karadag, "Design of metasurface polarization converter from linearly polarized signal to circularly polarized signal," *OPTIK*, Vol. 161, 12–19, 2018.
18. HFSS version 14.0.1: High Frequency Structure Simulator Based on the Finite Element Method, [Online], Available: http://www.ansys.com.
19. Garg, R., P. Bhartia, I. Bahl, and A. Ittipiboon, *Microstrip Antenna Design Handbook*, 371–374, Artech House, Norwood, MA, USA, 2001.
20. Data Sheet of ROHDE&SCHWARZ ZVB20, Application Note, [Online], Available: http://www.rohde-schwarz.com/.